Bock, G. (1994): Multiples as precursors to S, SKS and ScS. - Geophysical Journal International, 119, 2, pp. 421—427.

DOI: https://doi.org/10.1111/j.1365-246X.1994.tb00132.x

Geophys. J. Int. (1994) **119**, 421–427

Multiples as precursors to *S*, *SKS* and *ScS*

Günter Bock
GeoForschungsZentrum, Telegrafenberg A6, 14473 Potsdam, Germany

Accepted 1994 March 21. Received 1994 March 18; in original form 1993 July 28

SUMMARY

Complete theoretical *P–SV* seismograms calculated for the radially symmetrical IASP91 model with the reflectivity method show a wide variety of seismic phases in the time window between *P* and mantle *S* at teleseismic distances. One particular phase, which appears as precursor to *S* mainly on vertical-component seismograms, clearly stands out over the distance range from 62° to 70°. If interpreted as an *S–P* conversion from upper mantle discontinuities, the lead time to mantle *S* of about 30 s would indicate a conversion depth of 220 km. Clearly, this would be a false interpretation because the IASP91 model does not contain a discontinuity at this depth. Synthetic seismograms calculated with the Gaussian beam method indicate that the precursors can be explained by superposition of *P* and *S* multiples between the surface and the transition zone from the upper to the lower mantle. Surface multiples of this kind appear as *S*-wave precursors, up to about 90° distance, and may have amplitudes that are comparable to those of *S–P* converted waves from the upper mantle transition zone. Interference between surface multiples and mode-converted phases may lead to highly variable amplitudes of *S*-wave precursors. An observation from the long-period Global Seismograph Network station NWAO (Narrogin, Western Australia) suggests that surface multiples are actually observed as precursors to *S*.

Key words: body waves, mantle discontinuities, synthetic seismograms.

INTRODUCTION

Mode-converted and reflected waves have provided important insights into the nature of seismic discontinuities located in the transition zone between upper and lower mantle, at depths between 400 and 700 km. An important class are *S–P* and *P–S* converted waves that appear as precursors to mantle *S*, *SKS* and *ScS* (Båth & Stefánsson 1966; Jordan & Frazer 1975; Sacks, Snoke & Husebye 1979; Faber & Müller 1980, 1984; Baumgardt & Alexander 1984; Bock & Kind 1991). They are often easy to identify on seismograms of single stations.

An important aspect of data interpretation in studies of *S–P* and *P–S* converted waves is that *P* surface multiples may also appear with significant amplitudes in the time window prior to *S* (e.g. Sacks *et al.* 1979). For shallow-focus events, multiples like *PP*, *PPP*, *P4*, etc., and associated depth phases have sufficiently decayed in amplitude in the time interval prior to *S* where *S–P* converted phases from mantle discontinuities are expected to arrive (Faber & Müller 1980). This is the main reason why data from shallow-focus earthquakes are normally used in studies of mode-converted waves that appear as precursors to *S*. However, multiples other than *P* surface reflections have never been explicitly mentioned in the studies just cited. Shearer (1990, 1991) has shown that a variety of multiples may show up that are caused by repeated reflections between the surface and the upper mantle transition zone. It is the aim of this note to point out that higher-order multiples of this kind may reach significant amplitudes and may appear in the same time window as *S–P* conversions from the upper mantle. Consequently, great care should be taken not to confuse these phases. The best and probably only way to avoid false interpretations is to check observations with the help of complete synthetic seismograms that can be calculated, for example, with the reflectivity method (e.g. Müller 1985).

THEORETICAL *P–SV* SEISMOGRAMS

Figure 1 shows a theoretical seismogram section (vertical component) calculated with the reflectivity method for a shear dislocation point source (Kind 1979) at 10 km depth for the IASP91 model (Kennett & Engdahl 1991). Seismograms are convolved with the SRO instrument response. The dominant period is 25 s, which corresponds to a wavelength of about 125 km. Long-period seismograms permit only limited resolution of the sharpness of seismic

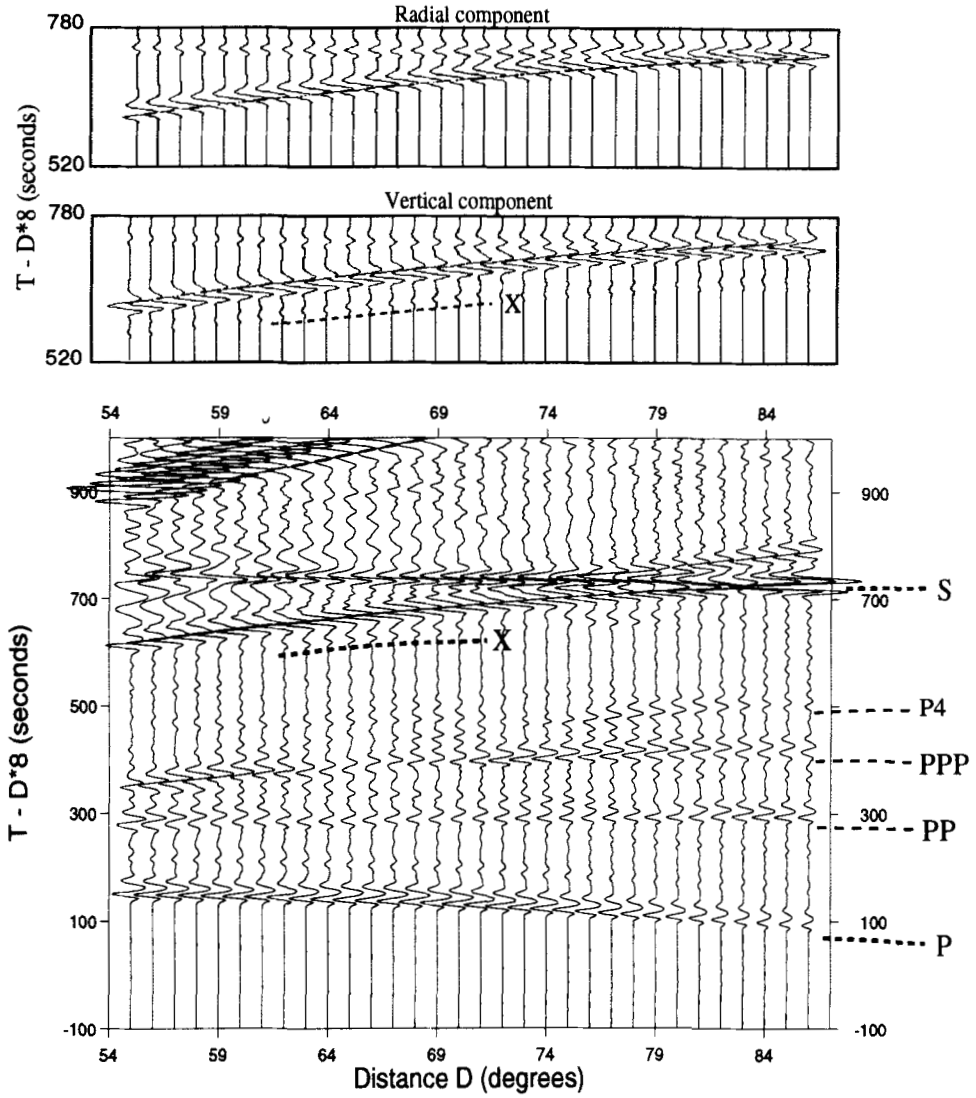

Figure 1. Bottom panel: synthetic seismogram section (vertical component) calculated with the reflectivity method for a point source at 10 km depth. A dip-slip mechanism is assumed with the fault plane dipping at 70° toward the receivers. *P* surface multiples *PP*, *PPP* and *P*4 are visible between about 300 and 500 s reduced time. The label *S* comprises the phases *S*, *SKS* and *ScS*. Phase *X* represents a multiple between surface and mantle transition zone. Top panels: Gaussian beam synthetics (vertical and radial-horizontal components) plotted for the time interval between 520 s and 780 s reduced time.

discontinuities. A shear dislocation dip-slip point source was assumed in all calculations with the fault plane dipping at 70° toward the receivers. This source orientation is particularly favourable to producing strong *S–P* conversions from upper mantle discontinuities beneath the receivers that appear as precursors to mantle *S*, *SKS* and *ScS* mainly on vertical-component seismograms (Faber & Müller 1984). *P–S* converted waves that have their conversion points beneath the source and that would appear mainly on radial-horizontal seismograms have negligible amplitudes in this case. As noted by Faber & Müller (1984), other source mechanisms will normally cause interference between *S–P* and *P–S* conversions such that precursors have larger amplitudes on the radial-horizontal than on the vertical-component seismograms. The latter case is not investigated in this paper.

The surface reflections *PP*, *PPP* and *P*4 are clearly visible in the *P*-wave coda (Fig. 1). Phases preceding *S* by about 50 s begin to appear at distances beyond 75° where their traveltimes are compatible with *S–P* conversions from the 410 km discontinuity. An interesting point is that these precursors are not continuous in amplitude over the range $75° \leq \Delta \leq 86°$. It will later be shown that this is the result of constructive and destructive interference between *S–P* conversions from the transition zone and multiples between the surface and the transition zone. Another phase, termed *X* in the following, also has the polarity of the *P* wave. It precedes *S* by about 30 s and has appreciable amplitudes at distances between about 60 and 72°. In a radially symmetrical earth, this is the distance range over which mode conversions from *S* to *P* occurring in the upper mantle at depths between about 80 and 220 km may produce *S* precursors of significant amplitude (Sacks *et al.* 1979). However, the IASP91 model has no seismic discontinuities in

this depth interval. Therefore, other causes for phase X should be considered.

A possible explanation for X is that it is built up by a number of multiples between the surface and the transition zone from the upper to the lower mantle. Multiples that have the correct arrival time of X consist of a single S-wave reflection from the 660 km discontinuity and three P-wave surface reflections (i.e. phases *s660sPPP*, *Ps660sPP*, *PPs660sP*, and *PPPs660s*). Other multiples consisting of three P-wave legs and a single reflection from the 410 km or 660 km discontinuity (involving P–S, S–P and P–P reflections) arrive much earlier than X; therefore, they could hardly be mistaken for S–P converted phases from upper mantle discontinuities.

The lead times of *s660sPPP*, *Ps660sPP*, etc., relative to S vary from about 20 s to 75 s over the distance range $50° \leq \Delta \leq 100°$ (Fig. 2). The traveltime curve in Fig. 2 shows two triplications that are associated with the 410 km and 660 km discontinuities. Possible ray paths of the multiple are shown in Fig. 3 for the earth-flattening approximation (Müller 1977) of the IASP91 model and an epicentral distance $\Delta = 65°$. At this distance, the P-wave legs are associated with five different ray paths through the upper mantle, which are illustrated in Fig. 3. For each ray path of P, four different combinations of the P- and S-wave legs are possible, depending on the location of the S-wave leg. The traveltimes of the corresponding multiples are approximately the same, leading to constructive interference on long-period seismograms at the receiver. In Fig. 3, only the paths of the multiples which have the S-wave reflection beneath the source are shown.

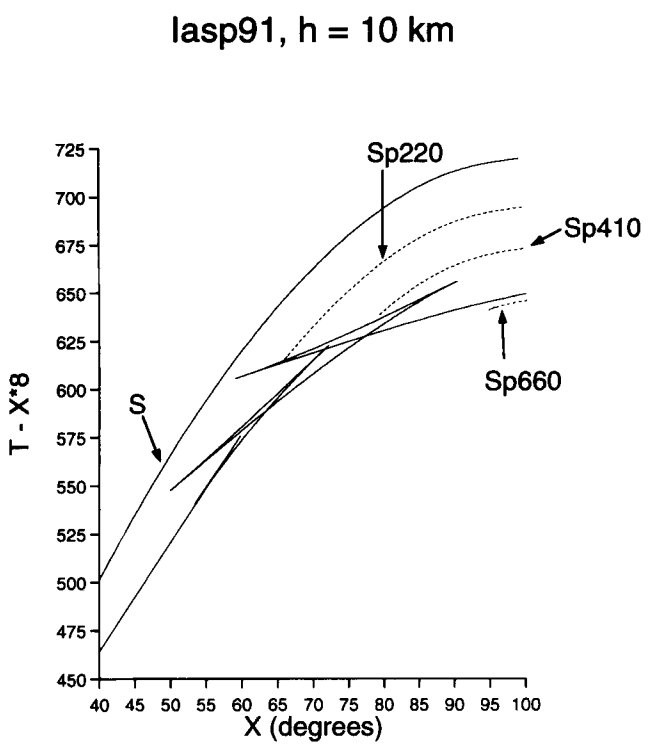

Figure 2. Traveltime curve for mantle S and multiples between surface and upper mantle transition zone (solid lines), and S–P converted phases at 220 km, 410 km and 660 km depth (dashed lines).

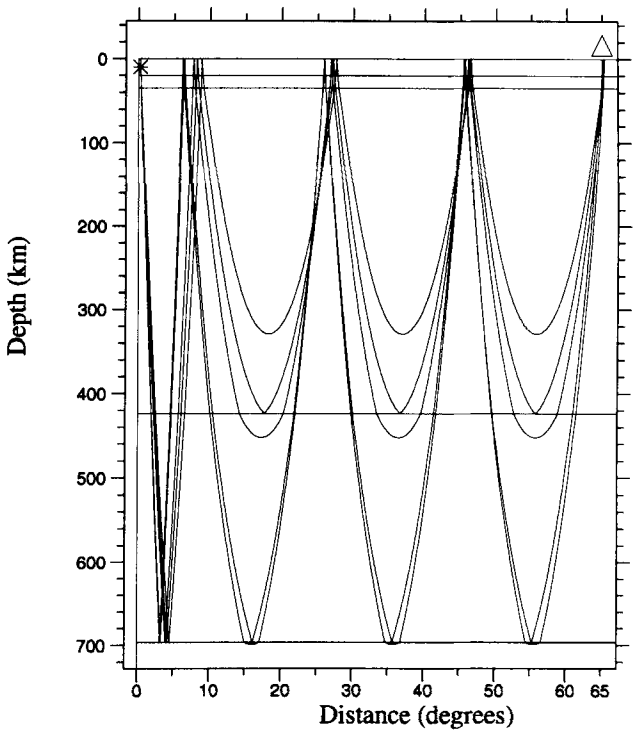

Figure 3. Ray path geometry of the multiples for which Gaussian beam seismograms are shown in Fig. 4. Epicentral distance is 65°. Each multiple consists of one S-wave reflection from the 660 km discontinuity (only the combination which has the S-wave leg beneath the source is shown here) and three P-wave surface reflections that travel to this distance along five different paths through the mantle due to triplications in the traveltime curve. The '410 km' and '660 km' discontinuities appear at greater depths in the earth-flattening approximation of the spherical earth model. Four different ray path combinations are possible depending on the position of the S-wave leg; the corresponding phases have approximately the same traveltimes.

GAUSSIAN BEAM SYNTHETICS

The Gaussian beam method as implemented by Weber (1988) and Davis & Henson (1993) was used to determine whether multiples of this kind contribute sufficient energy in the time window prior to S. The method offers the advantage that the amplitudes of seismic phases along specified ray paths can be investigated. The results of these calculations are shown in Fig. 1 and Figs 4–6. The calculations were carried out for S, *SKS*, *ScS*, S–P, *SKS*–P and *ScS*–P conversions from the 410 km and 660 km discontinuities, and all possible combinations of the multiple *s660sPPP*. It is obvious from Figs 2 and 3 that, at some distances, possible P-wave legs of the multiples follow five different paths through the mantle. All these paths are considered in the Gaussian beam synthetics. Depth phases of the type sX were also included, with X denoting here all the above phases. The depth phases pX had small amplitudes for the chosen source orientation and were therefore omitted from the Gaussian beam calculations.

Multiples of the type *s660sPPPP*, consisting of a single S-wave reflection from the 660 km discontinuity and four P-wave surface reflections, may also appear prior to S.

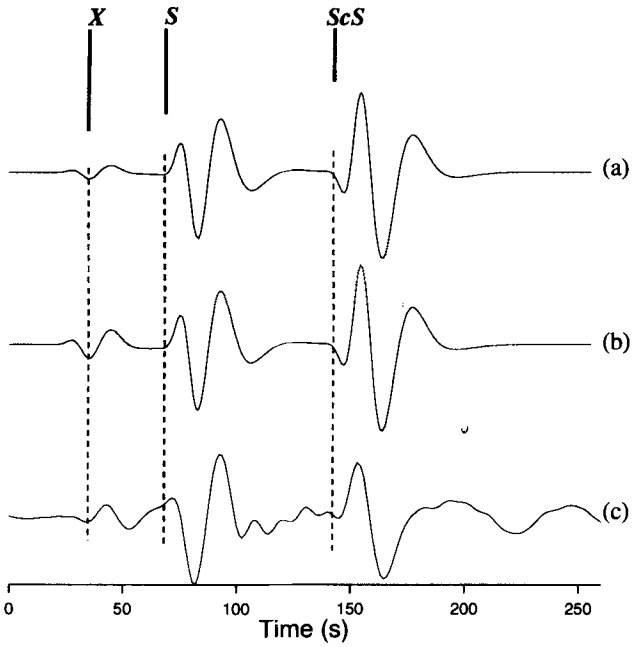

Figure 4. Synthetic seismograms calculated with the Gaussian beam (a and b) and reflectivity method (c) for the dislocation source described in Fig. 1, for an epicentral distance $\Delta = 65°$. The *S*-wave precursors marked by *X* in trace (a) are formed by multiples consisting of a *P*-wave leg beneath the source followed by a single *S*-wave reflection from the 660 km discontinuity and two more *P* surface reflections. In trace (b) all possible combinations of multiples as described in the text were considered. For an illustration of the ray path geometry see Fig. 3.

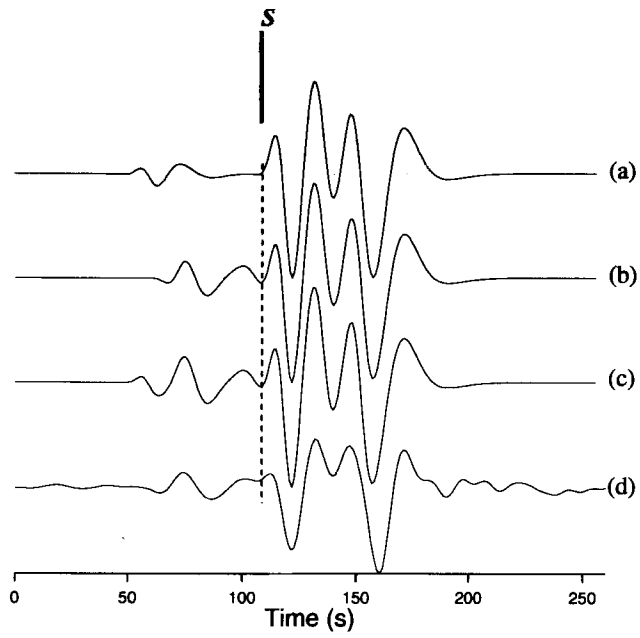

Figure 5. Gaussian beam (a, b and c) and reflectivity (d) synthetics for $\Delta = 77°$. *S*-wave precursors are built up from (a) multiples between the surface and upper mantle transition zone, and (b) from *S–P* conversions from the transition zone. Superposition of (a) and (b) leads to constructive interference between these phases (trace c).

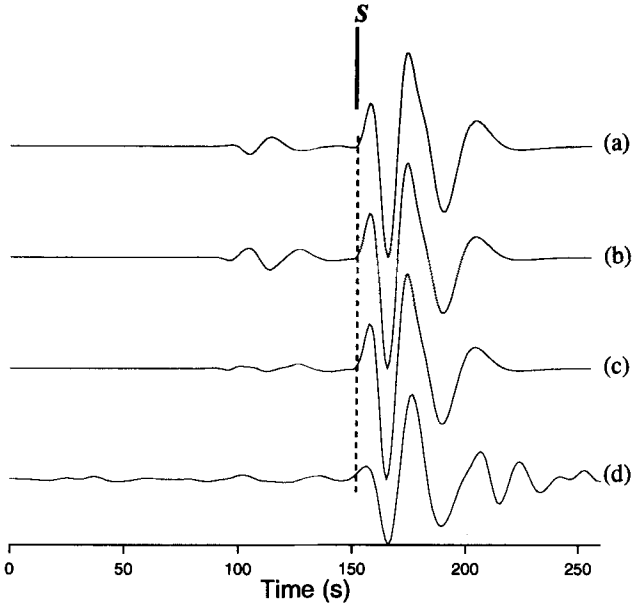

Figure 6. Same as Fig. 5, but for $\Delta = 81°$. At this distance, multiples and *S–P* converted phases interfere destructively resulting in very small *S*-precursors.

However, their amplitudes in the distance range between 60° and 72° are small and do not match those of phase *X*.

Gaussian beam synthetics are plotted as record section in the upper two panels of Fig. 1. The *S*-wave precursors in the Gaussian beam seismograms have their main energy on the vertical component, which is in good agreement with the reflectivity synthetics. Also, the range-dependent behaviour of the precursors agrees reasonably well with the reflectivity seismograms. In the following, a more detailed comparison between reflectivity and Gaussian beam synthetics is made at three specific distances. Only the vertical-component seismograms are shown because it is in these that the effects are best seen.

Superposition of multiples having differing paths but similar arrival times may lead to constructive interference of the precursor phase. This is obvious by comparison between the middle and top trace in Fig. 4. The top trace shows the Gaussian beam synthetic for a precursor of the type *Ps660sPP* (i.e. one *P* leg beneath the source, followed by the single *S* reflection from the 660 km discontinuity and two more *P* surface multiples with the *P* legs bottoming between 410 and 660 km depth). The precursor amplitude is considerably smaller than in the middle trace of Fig. 4 which incorporates all possible combinations of the multiples. *S–P* converted phases from the 410 km and 660 km discontinuities contribute in this example negligible energy to the time intervals prior to *S*.

Figures 5 and 6 illustrate examples in which *S–P* conversions at the upper mantle transition zone provide significant precursor amplitudes prior to *S*, *SKS* and *ScS*. They do interfere with multiples of the type just discussed; constructively in the example of Fig. 5, and destructively in that of Fig. 6.

In all Gaussian beam calculations, option 9 for the complex beam parameter ε was used as described by Weber (1988). The ε depends on the size of the triangles that are

used to discretize the model. The results presented in Figs 4–6 were obtained for a grid which consisted of 35 knot points over 100° horizontal distance. This produced precursor amplitudes relative to *S* that match those in the reflectivity synthetic quite well. Clearly, the reflectivity synthetic is likely to give a better approximation of the complete wavefield than the Gaussian beam method. For example, shear-coupled *PL* phases in the *S*-wave coda that are included in the reflectivity seismograms are not modelled by the Gaussian beam method.

Notwithstanding the questions about the completeness of the Gaussian beam synthetics, the important point is that the results offer a model for the *S*-wave precursors seen in the reflectivity synthetics. Comparison of the Gaussian beam with the reflectivity synthetics suggests that the *S*-wave precursor can indeed by explained by interference of multiples between the surface and the upper mantle transition zone and *S–P* converted waves. In the example of Fig. 4, the contribution from *S-P* converted phases to the *S*-wave precursors is small compared to that from the surface multiples. In this case, the precursors can be reasonably well explained by superposition of multiples between the surface and the upper mantle transition zone alone.

A necessary condition for the presence of the multiples seems to be the existence of a 'sharp' 660 km discontinuity. By 'sharp' we mean that the transition must take place over a depth interval which is less than about a quarter of the wavelength or about 30 km. This is consistent with recently published results (Petersen *et al.* 1993) on the sharpness of mantle discontinuities. Replacing the IASP91 660 km discontinuity by a smooth transition was sufficient to reduce the multiples to the extent that they became invisible in reflectivity synthetic seismogram sections. However, the amplitudes of the multiples are not so sensitive to the sharpness of the 410 km discontinuity. They are still clearly seen in the synthetics if the IASP91 410 km discontinuity is replaced by a smooth transition. This is related to the fact that the multiples built up by *P* waves bottoming between the 410 km and 660 km discontinuities contribute most of the precursor energy.

The examples of Fig. 1 and Figs 4–6 sound a word of warning, namely, that interpreting *S*-wave precursors in terms of *S–P* conversions from upper mantle discontinuities alone may lead to false conclusions. Slowness measurements might offer a way to discriminate between surface multiples and mode-converted phases at distances where the slownesses are sufficiently different. However, most data used for the study of *S–P* conversions from the mantle come from long-period single stations of the GSN inhibiting slowness analyses.

AN OBSERVATIONAL EXAMPLE

Figure 7 shows a long-period seismogram of an earthquake at Ryukyu Island recorded at the Global Seismographic Network station NWAO (Narrogin, Australia). An *S*-wave precursor is clearly seen on the vertical and radial-horizontal components. It has a *P*-wave type of polarization and a lead time to *S* of about 30 s. Initially, the author thought of this and other similar observations at NWAO as a good example

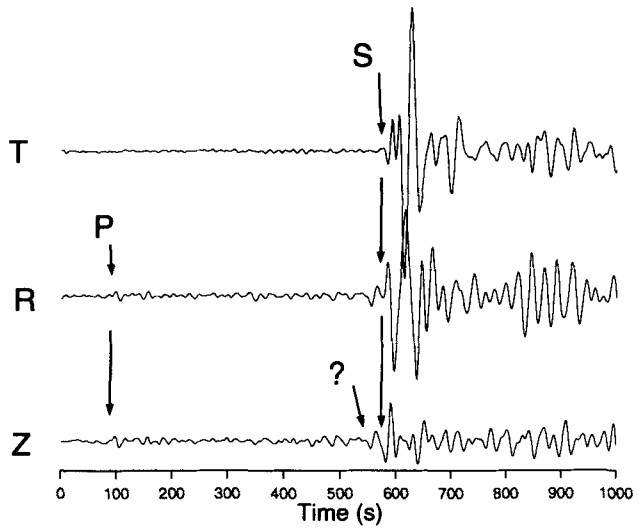

Figure 7. Long-period NWAO seismograms (vertical (Z), radial (R) and transverse-horizontal (T) components) of an earthquake at Ryukyu Island (ISC source data: origin time 1984 July 19, 23:25:12.1 UTC, location 28.11°N, 129.52°E, depth = 44 km from *pP*) at an epicentral distance $\Delta = 61.8°$. The records shown start at 23:34:19.9 UTC. A precursor to *S* marked by a question mark is visible on the Z and R components.

of an *S–P* conversion from the 220 km discontinuity which is a prominent feature of the PREM model (Dziewonski & Anderson 1981). However, this interpretation had to be discarded when the observations were compared with complete synthetic seismograms calculated with the reflectivity method for the PREM and IASP91 models (Fig. 8). No attempts were made to improve the poor match between observed and synthetic waveforms of the *S*-wave coda. The important point is that the IASP91 model provides a more satisfactory fit to the observed *S*-wave precursor than the PREM model. Therefore, it cannot be ruled out that the precursor is caused by a superposition of multiples as discussed in the previous section. The discrepancy between the observed and theoretical amplitudes of the *S*-wave precursor may result from the fact that the travel path from source to receiver traverses different tectonic regions, causing an interference pattern that cannot be correctly modelled by the rerflectivity synthetics. Note that the *S*-wave precursor has appreciable amplitudes not only on the vertical, but also on the radial-horizontal component of both observed and synthetic seismograms.

DISCUSSION

The previous examples illustrate the importance of considering all possible phases including multiples in the interpretation of *S*-wave precursors. Even in the seemingly 'simple' case of a radially symmetrical earth, a large variety of multiples may be generated by repeated reflections/refractions between the surface and seismic discontinuities in the mantle. Some of these multiples appear as precursors to *S* and may be easily mistaken for *S–P* converted phases. Interference of surface-transition zone multiples with *S–P* conversions from the transition zone may drastically alter the amplitudes of *S–P* converted

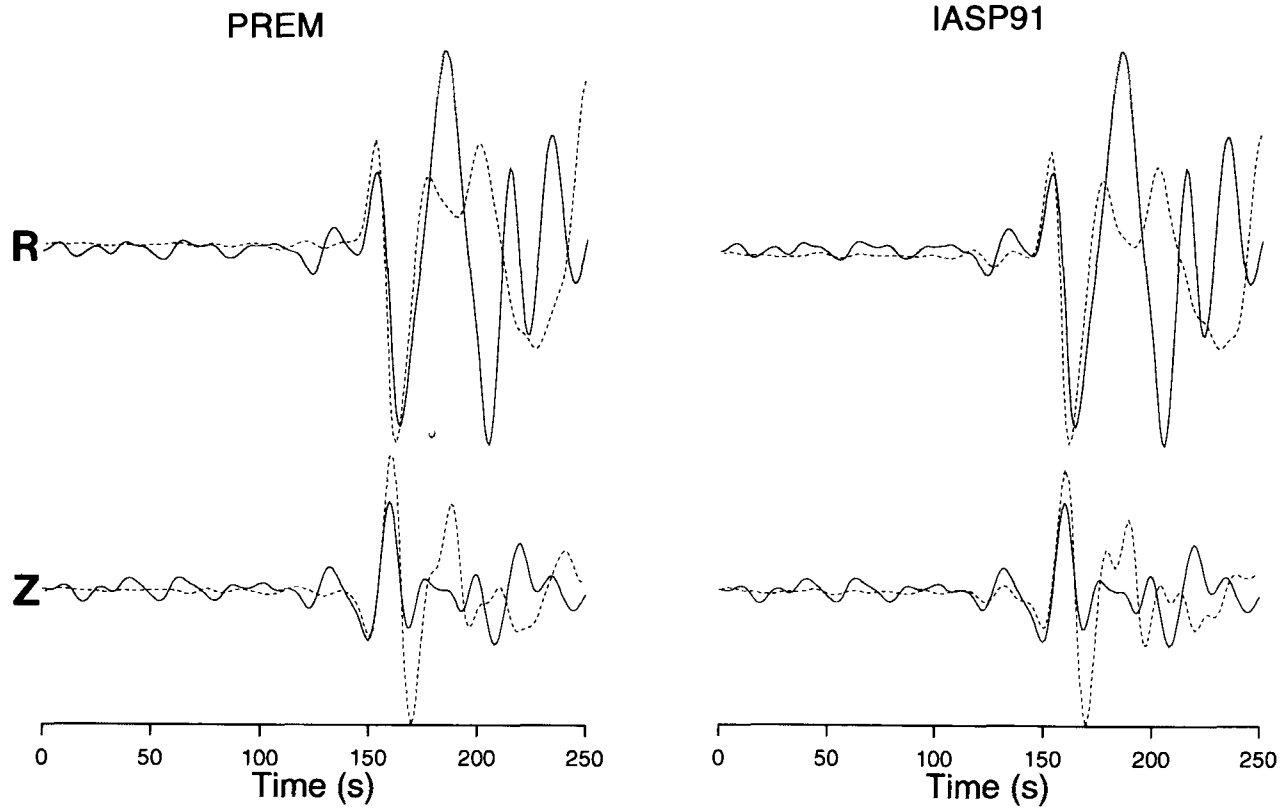

Figure 8. Comparison of a 250 s long part of the Z and R component of the recordings shown in Fig. 7 (solid lines), which includes *S* and *S*-wave precursors, with reflectivity synthetics (dashed lines) for the PREM and IASP91 models, source depth = 44 km. The fault plane parameters used are: strike = 2°, dip = 66°, rake = 161°, from the Harvard CMT solution.

waves. This makes it difficult to obtain an unbiased estimate of the velocity contrast across the discontinuities from the observed precursor-to-*S* amplitude ratio. The degree of interference is difficult to predict with radially symmetrical earth models because traveltimes and amplitudes of the multiples will be modified by regional variations in upper mantle structure between source and receiver. Scattered waves in laterally varying media not modelled by the reflectivity synthetics also contribute to the wavefield.

The question arises whether previously reported observations of mode-converted phases preceding *S* could represent multiples in a radially symmetrical earth. Here, I focus on the studies of Sacks *et al.* (1979) and Bock (1991) who gave estimates of the depth to the asthenosphere–lithosphere boundary (ALB) based on *S–P* converted phases. They estimated depths of 250 km beneath the Baltic shield (Sacks *et al.* 1979) and 75 km below the Hawaian island of Oahu (Bock 1991). IASP91 reflectivity synthetics were calculated for the events used by these authors. Event 1 from Sacks *et al.* (1979) was the only one for which the synthetics predict virtually no visible energy in the interval preceding *S*. In all the other cases, clear *S* precursors were seen on the theoretical seismograms. In contrast to *S–P* converted phases, however, they have variable lead times relative to *S* which is related to the fact that many events having different focal depths and epicentral distances were used. This is an important point because there is no consistent precursor pattern emerging if the synthetics are aligned on mantle *S*, in sharp contrast to the observed *S*-wave precursors that exhibit constant lead times to *S* over a wide distance interval and a range of focal depths. This is the main argument to support the interpretation of both Sacks *et al.* (1979) and Bock (1991), namely, that the observed precursors were correctly identified as *S–P* converted phases from the ALB.

CONCLUSIONS

Precursors to teleseismic *S* waves are frequently observed on the vertical and radial-horizontal components of long-period seismograms. A common interpretation of these phases is that they represent *S–P* converted waves from upper mantle discontinuities. Synthetic seismogram modelling suggests, however, that *S*-wave precursors may also be produced by higher-order multiples between the surface and the upper mantle transition zone. Such multiples have not been explicitly discussed, to the best of the author's knowledge, in papers dealing with *S–P* converted waves from the upper mantle. They appear over a wide distance range with amplitudes comparable in size to those of *S–P* conversions from the upper mantle transition zone. Interference of mode-converted and multiple phases may lead to considerable variations in the amplitudes of precursors to teleseismic *S*, *SKS* and *ScS*. Interpretation of these precursors in terms of *S–P* conversions alone may therefore lead to erroneous estimates for velocity contrasts across, and depths to, mantle discontinuities. In the examples shown for

radially symmetrical earth models, amplitudes of multiples dominate those of $S-P$ converted phases from the transition zone at smaller epicentral distances, about $62° \leq \Delta \leq 71°$.

Great care must be taken not to misinterpret these S-wave precursors as mode-converted phases from the upper mantle. At larger distances superposition of multiples with $S-P$ converted waves from the mantle transition zone between 400 and 700 km may lead to constructive or destructive interference in the resulting waveform.

There are two ways to avoid pitfalls in the interpretation of mode-converted phases preceding S. First, one has to use a data base covering a wide distance range and including events over a range of focal depths. Mode-converted waves will have constant lead times relative to S while multiples will not. Secondly, the observations should always be compared with synthetics of the complete wavefield. For example, the reflectivity method allows us to calculate complete synthetic seismograms for radially symmetrical earth structures; these synthetics should always be compared with observed S-wave precursors. This may help to avoid false interpretations of S-wave precursors in terms of structure. To test whether observed precursors may result from $S-P$ conversions, synthetics should be calculated both for a model with a seismic discontinuity at the appropriate depth of conversion and without it. If precursors are prevalent in both calculations, the interpretation that they are caused by $S-P$ conversion beneath the receiver must be discarded. Other causes may then be investigated by different methods, e.g. the Gaussian beam method.

ACKNOWLEDGMENTS

I am particularly indebted to Chuck Estabrook who introduced me to the XY and ICE postscript plotters written by Paul Wessel and Roger Davis, respectively, of the Lamont–Doherty Earth Observatory. I thank Chuck Eastabrook and Rainer Kind for critically reading the manuscript.

REFERENCES

Båth, M. & Stefánsson, R., 1966. $S-P$ conversion at the base of the crust, *Ann. Geofis.*, **19,** 119–130.

Baumgardt, D.R. & Alexander, S.S., 1984. Structure of the mantle beneath Montana LASA from analysis of long-period, mode-converted phases, *Bull. seism. Soc. Am.*, **74,** 1683–1702.

Bock, G., 1991. Long-period S to P converted waves and the onset of partial melting beneath Oahu, Hawaii, *Geophys. Res. Lett.*, **18,** 869–872.

Bock, G. & Kind, R., 1991. A global study of S-to-P and P-to-S conversions from the upper mantle transition zone, *Geophys. J. Int.*, **107,** 117–129.

Davis, J.P. & Henson, I.H., 1993. User's guide to Xgbm: An X-Windows system to compute Gaussian beam synthetic seismograms, *Report TGAL-93-02,* Teledyne Geotech Alexandria Laboratories.

Dziewonski, A.M. & Anderson, D.L., 1981. Preliminary reference Earth model, *Phys. Earth planet. Inter.*, **25,** 297–356.

Faber, S. & Müller, G., 1980. *Sp* phases from the transition zone between the upper and lower mantle, *Bull. seism. Soc. Am.*, **70,** 487–508.

Faber, S. & Müller, G., 1984. Converted phases from the mantle transition zone observed at European stations, *J. Geophys.*, **54,** 183–194.

Jordan, T.H. & Frazer, L.N., 1975. Crustal and upper mantle structure from *Sp* phases, *J. geophys. Res.*, **80,** 1504–1518.

Kennett, B.L.N. & Engdahl, E.R., 1991. Traveltimes for global earthquake location and phase identification, *Geophys. J. Int.*, **105,** 429–465.

Kind, R., 1979. Extensions of the reflectivity method, *J. Geophys.*, **45,** 373–380.

Müller, G., 1977. Earth-flattening approximation for body waves derived from geometric ray theory—improvements, corrections and range of applicability, *J. Geophys.*, **42,** 429–436.

Müller, G., 1985. The reflectivity method: a tutorial, *J. Geophys.*, **58,** 153–174.

Petersen, N., Vinnik, L., Kosarev, G., Kind, R., Oreshin, S. & Stammler, K., 1993. Sharpness of the mantle discontinuities, *Geophys. Res. Lett.*, **20,** 859–862.

Sacks, I.S., Snoke, J.A. & Husebye, E.S., 1979. Lithosphere thickness beneath the Baltic shield, *Tectonophysics,* **56,** 101–110.

Shearer, P.M., 1990. Seismic imaging of upper mantle structure and new evidence for a 520 km discontinuity, *Nature,* **344,** 121–126.

Shearer, P.M., 1991. Constraints on upper mantle discontinuities from observations of long-period reflected and converted phases, *J. geophys. Res.*, **96,** 18 147–18 182.

Weber, M., 1988. Computation of body-wave seismograms in absorbing 2-D media using the Gaussian beam method: comparison with exact methods, *Geophys. J.*, **92,** 9–24.